



**HAL**  
open science

## Energy management and sizing algorithm applied on a hybrid power system supplying an isolated residential application

Ramzi Saidi, Jean-Christophe Olivier, Mohamed Machmoum, Eric Chauveau

► **To cite this version:**

Ramzi Saidi, Jean-Christophe Olivier, Mohamed Machmoum, Eric Chauveau. Energy management and sizing algorithm applied on a hybrid power system supplying an isolated residential application. IECON 2018, Oct 2018, Washington, United States. hal-01928890

**HAL Id: hal-01928890**

**<https://hal.science/hal-01928890>**

Submitted on 7 Dec 2018

**HAL** is a multi-disciplinary open access archive for the deposit and dissemination of scientific research documents, whether they are published or not. The documents may come from teaching and research institutions in France or abroad, or from public or private research centers.

L'archive ouverte pluridisciplinaire **HAL**, est destinée au dépôt et à la diffusion de documents scientifiques de niveau recherche, publiés ou non, émanant des établissements d'enseignement et de recherche français ou étrangers, des laboratoires publics ou privés.

# Energy management and sizing algorithm applied on a hybrid power system supplying an isolated residential application

R.Saidi, J.C.Olivier, M. Machmoum

IREENA, University of Nantes  
Saint Nazaire, France  
ramzi.saidi@etu.univ-nantes.fr

Eric Chauveau

Département d'Electronique et Automatique  
ESEO-Tech, IREENA  
Angers, France  
eric.chauveau@eseo.fr

**Abstract**— This paper presents an energy management algorithm to be embedded for a residential application disconnected from the power grid. The multisource system studied includes solar panels as a renewable energy source, a fuel cell as a secondary source, three batteries and a bank of supercapacitors as storage systems. The proposed algorithm uses as input data, future estimates obtained from power consumption and meteorological forecasting data, and historical of the load power and the renewable power obtained from measurements. It is assumed that these two input powers are imposed and uncontrollable. In the case where the future estimates have errors compared to what has actually been measured, a mathematical approach shows that the algorithm is able to compensate these forecasting errors by sharing them between the different sources of the system while respecting their different characteristics. In addition to the optimal energy distribution, the algorithm gives the optimal size of each source and storage devices. In this work, the total cost of the system is chosen as the criteria to be optimized. The simulations are carried out over a year, with a time step of 1 second and in the presence of significant forecasting errors. The results obtained are particularly convincing and make it possible to validate this energy management strategy.

**Keywords**—energy management; centered moving average filters; forecasting errors; power forecasting

## I. INTRODUCTION

Nowadays, multisource production systems represent a major challenge for the energy production and transport industries. Thanks to these systems, the supply of isolated applications has become possible. In addition, these systems are often based on one or more sources of clean energy such as renewable energies or hydrogen, which makes their studies more and more interesting as the world tends to decrease the exploitation of conventional energy production systems such as power plants or combustion engines, because of the harmful effect they generate on the environment. These multisource systems can contain several energy sources of different characteristics. Indeed, the presence of several sources in a multisource system increases its lifetime and its reliability and on another hand avoids the complete shutdown of the system in case of malfunction of one of its sources [1].

Moreover, during the lifetime of the power system, one or more devices can be subject to replacement, or even substituted by new more efficient technologies. Then, it may be interesting that the architecture of these multisource systems was flexible and adaptable.

The distribution of the energy between the different devices and the fed load follows a set of laws that are called energy management strategies (EMS). But the coupling of several energy devices in the same production system makes the arbitrage and the management of energy flows more complex. This is partly one of the reasons why several authors limit their system to one or two sources associated with a single storage organ, thus making the system less complex and with limited degrees of freedom.

In fact, many authors use dynamic programming (DP) as EMS [2]. It is a very efficient technique and well adapted to energy management. It consists of sampling the power margin of the devices in  $n$  states and sampling the time axis in  $k$  stages and it is up to the algorithm to determine the optimal system state at each stage. As a result, the more the number of sources increases, the more the number of states multiplies and a multidimensional resolution grid is created, thus making the search time of the optimal paths very long, especially as soon as the number of paths to be optimized exceeds two or three. Other authors use fuzzy logic (FL) to share energy between the sources of the system [3], [4]. For this technique, a large number of sources cause a large number of membership functions, which also makes difficult the definition of the different rules.

Other works such as [5] are based on predictive control. This method is particularly effective for taking into account resource forecasting and usage profiles. This technique requires linear modeling of each device to be effective, which means that some important non-linear phenomena have to be neglected. Finally, the frequency separation is one of the most used EMS thanks to its ability to control sources by power profiles that go with their respective dynamics [6], [7], [8].

The work proposed in this article is in the framework of this last technique. Indeed, the proposed strategy is based on the cascading and paralleling of Centered Moving Average

(CMA) Filters that generate all the reference profiles to the system [3],[16]. The principle of the strategy appears applicable on a system composed of many energy sources. But instead of considering only cascaded filters, with a classical decomposition from low to high frequency ranges, we propose here to extend this idea to more general control architecture, with serie-parallel filters. This new control architecture permits to easily include different technologies of devices, on the one hand to ensure an optimal technical solution, and on the other hand to allow redundancy which improve the global reliability of the system. In addition to the optimal management of energy, the proposed algorithm allows to size these devices in such a way to minimize the total cost of the multisource system. The choice of the total cost of the system as the variable to be optimized, is explained by the fact that with this cost, we can evaluate the effect of several phenomena that the multisource system undergoes as for example aging, lifetime, maintenance, replacement and acquisition. In other words, the final cost of the system will reflect the total cost of one kWh produced.

This paper is organized as follows: Section II describes the architecture of the multisource production system. Section III presents the proposed algorithm applied to the multisource production system. Section IV presents the objective of optimization chosen in this study. The simulation results using predicted power profiles are presented in Section V. Finally, Section VI presents main conclusions of this paper.

## II. MULTISOURCE SYSTEM DESCRIPTION

Figure 1 shows the architecture of the studied hybrid system. It includes photovoltaic (PV) panels as a renewable energy source, a fuel cell (FC) as a secondary energy source, two batteries Li-ion, a lead acid battery and a bank of supercapacitors (SC) as energy storage systems (ESS). With the exception of PV panels, dimensions of all sources are not fixed. For the renewable source, 10 m<sup>2</sup> of PV panels are used. The DC / DC converters associated with PV panels and the FC are unidirectional Boost converters. On the other hand, for ESS, Buck-Boost bidirectional DC / DC converters are used to enable their charging and discharging phases. A negative power corresponds to a charging phase whereas a positive power corresponds to a discharge phase.

The representation of sources in this work has remained restricted on classical empirical models.

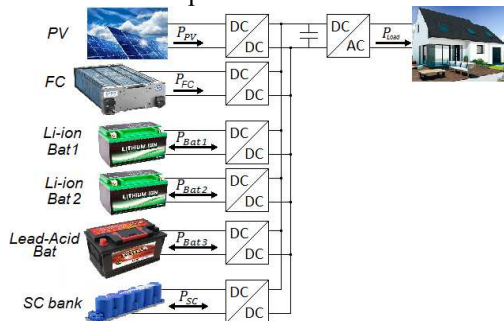


Fig. 1. Architecture of the studied multisource system.

The studied habitat is supposed located at Saint-Nazaire, France. For the estimation of the PV power profile  $\hat{P}_{PV}$ , a solar

profile generator has been developed and is presented in [9]. This generator based on the Markov matrix, generates an estimation of the radiation profile according to the geographical coordinates of the studied location (latitude / longitude), the inclination angle of PV panels and a sampling step. The PV power profile used in this study corresponds to the inputs shown in Table 1:

Table 1. Inputs of the solar profile generator..

Inputs	Value
Position (decimal degrees)	Saint Nazaire, France X: 47,283329 Y: -2,2
PV panels inclination (deg)	50
Sampling step (s)	1
Hs:Simulation horizon (year)	1

In addition, an estimated domestic load demand profile  $\hat{P}_{Load}$  was generated by a consumption profile generator algorithm that operates according to probabilities of load appearance along the day. This profile corresponds to the power consumption of 5 persons. It is assumed that the habitat does not include an electric heater but rather a refrigerator, lighting, an oven, a washing machine, a dishwasher and multimedia. Figure 2 shows the used load profile on three different time scales. These representations show that the more the time horizon considered decreases the more the dynamics of the load profile stabilizes. In other words, we can consider that the more the energy source dynamic is slow, the more its reference power on the reduced time horizons is stable and also vice versa. From these last considerations, an algorithm based on a multi-time horizons operation is developed.

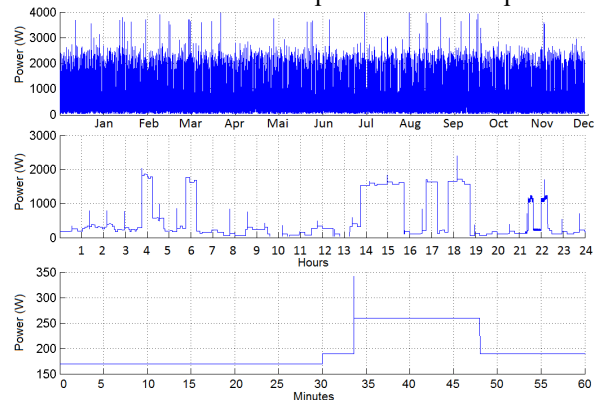


Fig. 2. Representation of the requested power profile on different time scales.

## III. ENERGY MANAGEMENT ALGORITHM

The proposed energy management algorithm is based on cascading/paralleling of several blocks called device-controllers, as shown in Figure 3. The total number of controllers is equal to the number of sources in the system. Each controller calculates, in real time, the reference power that a corresponding energy source must supply/store. In fact, at each instant  $t$ , it has at its input a set of *estimated future power values* and a set of *past power values* taken from a data history [9]. Based on these two future and past inputs, it gives the good reference power that its corresponding source has to supply/store at the present moment  $t$ . The proposed algorithm, illustrated in Figure 3, has for main input, two vectors  $\hat{\Delta P}$  and  $\Delta P$ . Both represent the difference between the power

demanded by the load and the power produced by PV panels over a simulation horizon  $H_s$ :

$$\hat{\Delta}P_{H_s} = \hat{P}_{Load_{H_s}} - \hat{P}_{PV_{H_s}} \quad (1)$$

$$\Delta P_{H_s} = P_{Load_{H_s}} - P_{PV_{H_s}} \quad (2)$$

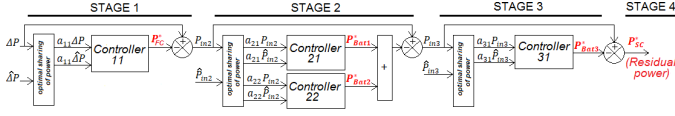


Fig. 3. Architecture of the proposed energy management algorithm.

The internal structure of a device controller is shown in Figure 4. It mainly comprises a Centered Moving Average (CMA) filter [3], [10] and safety devices (maximum powers (block in green), exceeding the SoC limits (block in red)).

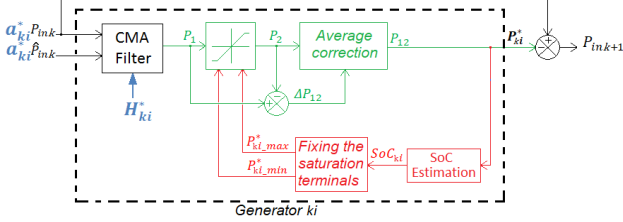


Fig. 4. Internal structure of a generator.

At each instant  $t$ , each filter calculates a centered average of its input vectors (future estimated vector and past measured vector) at a coefficient  $\alpha_{ki}^*$  near, over a well-defined time horizon  $H_{ki}^*$ . The mathematical relationship between the inputs and the output of each CMA filter at instant  $t$  is described as follows:

$$P_{ki}^*(t) = \frac{\alpha_{ki}^*}{H_{ki}^*} \int_{t-\frac{H_{ki}^*}{2}}^0 (2P_{in,k} - \hat{P}_{in,k}) dt + \frac{\alpha_{ki}^*}{H_{ki}^*} \int_0^{t+\frac{H_{ki}^*}{2}} \hat{P}_{in,k} dt \quad (3)$$

The output power expressions of filters are integral functions that connect the future to the past. In other words, these expressions relate past measured data that are always true, to predicted future data that may be erroneous. Taking into account the hypothesis (4), it becomes possible to say that the average of the output signal of each controller on  $H_s$ , is equal to that of its measured signal input:

$$\langle P \rangle_{H_s} = [\langle P \rangle_{H_k}]_{H_s} \quad \forall \quad H_k < H_s \quad (4)$$

This observation means that  $P_{FC}^*$ , the output power coming out of the first controller will have a mean value equal to the input vector  $\Delta P$ , what makes the average of  $P_{in,2}$ , the input power of the second controller, null and consequently, its outputs  $P_{Bat21}^*$  and  $P_{Bat22}^*$  also will have a zero-average on  $H_s$ . The same analysis is done for the two stages that come after. The zero-averages of  $P_{Bat21}^*$ ,  $P_{Bat22}^*$ ,  $P_{Bat31}^*$  and  $P_{SC}^*$  ensure that their respective States of Charge do not diverge along  $H_s$ .

The output power of a filter represents the first step in the construction of the reference power of the energy source. Each filter differs from the others by its time horizon  $H_{ki}^*$ . Indeed, the value of the time horizon of a filter depends on the dynamics of the source at which its output power is intended. The larger the time horizon, the smoother the filter output and *vice versa*. For this, the reference powers of slow dynamic sources must come from device-controllers containing filters operating with wide time horizons, while this time horizon can be smaller for fast sources. The coefficients  $\alpha_{ki}^*$  reflect the

maximum and minimum power level that the corresponding source can reach. Since the values of  $H_{ki}^*$  and  $\alpha_{ki}^*$  affect directly the output power of the device-controllers, the pairs  $(\alpha_{ki}^*, H_{ki}^*)$  play the role of the optimization variables in order to minimize the objective function described in the next section.

The main objective of the algorithm is to manage the measured unbalanced power  $\Delta P$  to ensure the equality between the power demand and the production. In other words, if the unbalanced power is positive, the controllable devices will supply power to the system, and on the other hand, if it is negative, the excess of power will be stored in the storage systems.

A difficulty is to propose control architecture able to handle a large number of devices (sources and storages) with very different characteristics (in power and energy densities).

To illustrate this problem, we propose to use an algorithm, which is inspired by frequency separation methods. Indeed, the cascade structure of the algorithm presents 4 stages according to the dynamics of the controlled energy sources. As for classical frequency separation, the first stage considers very high specific energy and low specific power (very slow source). On the other hand, the last stage (4<sup>th</sup>) consider very high specific power and low specific energy (very fast sources). Each other stage will be used to intermediary devices.

Indeed, among the five sources, the FC is the only source that is characterized by a high specific energy and a low specific power. As shown in Figure 3, this energy source will be controlled by the device-controller 11 placed on stage 1. Unlike FC, SC are storage devices that are characterized by high specific power and low specific energy. Then, their reference power must be a very high frequency profile. For this, this power is ensured by stage 4, which represents the *residual* power. Batteries are energy storage systems that are positioned between these last two devices. Without loss of generality, it is considered here one Lead-acid battery pack and two Li-ion batteries. According to the Ragone diagram [11], lead-acid batteries have a lower specific energy than Li-ion batteries. For this, the device-controllers of the stage 2 ensure power of the two Li-ion batteries. The stage 3 is then devoted for the Lead-acid battery.

Actually, as the proposed algorithm uses predicted values of load consumption and also solar radiation, these values may have deviations from the measured values. This difference is called forecasting error (FE)  $\varepsilon$ , defined as follows:

$$\hat{\Delta}P = \Delta P + \varepsilon \quad (5)$$

Indeed, with keeping the same assumption (4), by substituting the estimated power unbalance  $\hat{\Delta}P$  with equation (5), it appears an automatic error compensation term in the expression of each reference power. In fact, the profile of the forecasting error  $(\hat{\Delta}P - \Delta P)$  is automatically shared between the different sources while respecting the dynamics of each one. Equation (6) reflects the evolution of  $P_{FC}^*$  over time in presence of FEs. It presents an averaged term of forecasting errors. In other words, the FC automatically compensates the  $H_{11}^*$ -average value of this error over the horizon  $H_s$ :

$$P_{FC}^*(t) = \frac{1}{H_{11}^*} \left[ \int_{t-\frac{H_{11}^*}{2}}^{t+\frac{H_{11}^*}{2}} \hat{\Delta}P dt - 2 \int_{t-\frac{H_{11}^*}{2}}^t \varepsilon dt \right] \quad (6)$$

Where  $H_{11}^*$  is the optimal horizon of the FC corresponding filter. Indeed, the automatic correction provided by the FC consists of increasing or decreasing its reference power according to the sign of the average value of the error over  $H_s$  [16], [17].

As for the power profiles of the batteries and SC, the same phenomenon occurs. In fact, averaged terms of forecasting errors appear in the expressions of their reference powers. What is interesting in these results is that the sharing of this automatic compensation between the 5 sources of the system is done while respecting the dynamics of each source and also while keeping the average annual power of each ESS null, which guarantees the non-divergence of its SoC even in presence of forecasting errors. This previous finding is mathematically demonstrated in [16] and [17].

#### IV. OBJECTIVE OF OPTIMIZATION

The couples  $(a_{11}, H_{11})$ ,  $(a_{21}, H_{21})$ ,  $(a_{22}, H_{22})$  and  $(a_{31}, H_{31})$  of controllers 11, 21, 22 and 31 respectively, are optimized using *PSO* algorithm. These optimum values correspond to reference power profiles  $P_{FC}^*$ ,  $P_{Bat1}^*$ ,  $P_{Bat2}^*$ ,  $P_{Bat3}^*$  and  $P_{SC}^*$  which:

- respect the dynamics of the five sources of the system.
- respect the power limits of the five sources.
- respect the states of charge (SoC) of the storage systems.
- correspond to a minimum total cost of the system. This cost is explained below.

In this study, optimization is applied to the total cost of the system. This cost includes four components: the total initial cost, the total operation cost, the total replacement cost and the total maintenance cost. Given that these different costs are not evenly distributed over time and since the different sources do not have the same lifetimes, it will then be necessary to unify the period of time over which these costs will be calculated. In this case, the notion of annualized cost (cost per year) is used.

##### A. Devices lifetime

A degradation function  $\Delta_{FC}$  is considered for the FC. This function depends on its provided energy over the simulation horizon  $H_s$  [12]:

$$\Delta_{FC}(t) = \int_0^{H_s} \partial(t) dt \quad (7)$$

$$\text{Where } \partial(t) = \frac{\partial_0}{3600} \left[ 1 + \frac{\alpha}{P_{FC,nom}^2} (P_{FC}^*(t) - P_{FC,nom})^2 \right]$$

where  $\partial_0$ ,  $\alpha$  are coefficients and  $P_{FC,nom}$  the FC nominal power (80% of  $P_{FC,max}$ ). The degradation function  $\Delta_{FC}$  is expressed between 0 (beginning of life) and 1 (end of life). Once the degradation of the FC has been calculated, its lifetime is estimated as follows:

$$LT_{FC} = 1\text{year}/\Delta_{FC}(t = H_s)$$

The operation of a FC requires hydrogen. The consumption of this one is proportional to the energy provided by the FC. The volume  $V_{H2,ann}$  ( $m^3$ ) of the consumed hydrogen over a year is calculated as follows [13]:

$$V_{H2,ann} = (<P_{FC}^* >_{H_s} * H_s * 2.7778 \cdot 10^{-7}) / (3 * \eta_{FC})$$

With  $<P_{FC}^* >_{H_s}$  the average power supplied by the FC along the horizon  $H_s$  and  $\eta_{FC}$  the FC efficiency.

For batteries,  $\Delta_{Bat}$ , a function describing the evolution over time of their life. This evolution is proportional to the energy

that the battery exchanges compared to the maximum energy that it can exchange throughout its lifetime. Generally, a battery is able to perform a few thousand full charge/discharge cycles throughout its life.  $\Delta_{Bat}$  is expressed as follows [9]:

$$\Delta_{Bat}(t) = 1/(E_{Tot}) \int_0^{H_s} |E_{Exchanged}(t)| dt \quad (8)$$

With  $E_{Exchanged}$  the energy exchanged by the battery during  $H_s$  and  $E_{Tot}$  the total energy that it is able to exchange during its life. This energy is usually obtained by multiplying the storable energy by the maximum number of cycles. Once the equality  $|E_{Exchanged}| = E_{Tot}$  is verified, the battery reaches its end of life. The degradation function  $\Delta_{Bat}$  is expressed between 0 and 1. The estimated lifetime of the battery can then be calculated:

$$LT_{Bat} = 1\text{year}/\Delta_{Bat}(t = H_s)$$

$\Delta_{SC}$ , the degradation function of the SC bank [14], [15].  $\Delta_{SC}$  depends on the state of charge of the bank (SoCsc) :

$$\Delta_{SC}(t) = \int_0^{H_s} \partial(t) dt \quad (9)$$

$$\text{Where } \partial(t) = \frac{0,015}{3600 * 24 * 365} * 2^{12,5(\sqrt{SoCsc(t)} - 1)}$$

Thus, the estimated lifetime of the bank is deduced as follows:

$$LT_{SC} = 1\text{year}/\Delta_{SC}(t = H_s)$$

The renewable source generally has the longest lifetime among the sources of a multisource system. For this, the lifetime of a multisource system is generally equal to that of the renewable source present in this system. The lifetime of PV panels is estimated at 25 years.

##### B. Devices total costs

Taking into account the previous lifetimes, the annualized costs of each device are calculated [9], as shown in table 2.

Table 2. Annualized costs of each device of the studied multisource system.

<b>PV Panels</b>	
Annualized Initial cost	$\hat{C}_{init\ PV\ ann} = (\hat{C}_{inv\ PV} + 0.4 * \hat{C}_{inv\ PV})/25$
Annualized maintenance cost	$\hat{C}_{main\ PV\ ann} = 0.01 * \hat{C}_{init\ SC\ ann}$
Annualized total cost	$\hat{C}_{Tot\ PV\ ann} = \hat{C}_{init\ PV\ ann} + \hat{C}_{main\ PV\ ann}$
<b>Fuel cell</b>	
Annualized Initial cost	$\hat{C}_{init\ FC\ ann} = \hat{C}_{inv\ FC}/LT_{FC}$
Annualized operation cost	$\hat{C}_{Op\ FC\ ann} = V_{H2,ann} * Pr_{m3.H2}$
Annualized replacement cost	$\hat{C}_{rep\ FC\ ann} = 0.04 * \hat{C}_{init\ FC\ ann}$
Annualized maintenance cost	$\hat{C}_{main\ FC\ ann} = 0.04 * \hat{C}_{init\ FC\ ann}$
Annualized total cost	$\hat{C}_{Tot\ FC\ ann} = \hat{C}_{init\ FC\ ann} + \hat{C}_{Op\ FC\ ann} + \hat{C}_{rep\ FC\ ann} + \hat{C}_{main\ FC\ ann}$
<b>Battery</b>	
Annualized Initial cost	$\hat{C}_{init\ Bat\ ann} = \hat{C}_{inv\ Bat}/LT_{Bat}$
Annualized replacement cost	$\hat{C}_{rep\ Bat\ ann} = 0.03 * \hat{C}_{init\ Bat\ ann}$
Annualized maintenance cost	$\hat{C}_{main\ Bat\ ann} = 0.03 * \hat{C}_{init\ Bat\ ann}$
Annualized total cost	$\hat{C}_{Tot\ Bat\ ann} = \hat{C}_{init\ Bat\ ann} + \hat{C}_{rep\ Bat\ ann} + \hat{C}_{main\ Bat\ ann}$
<b>SC bank</b>	
Annualized Initial cost	$\hat{C}_{init\ SC\ ann} = \hat{C}_{inv\ Bat}/LT_{Bat}$
Annualized replacement cost	$\hat{C}_{rep\ SC\ ann} = 0.03 * \hat{C}_{init\ Bat\ ann}$
Annualized maintenance cost	$\hat{C}_{main\ SC\ ann} = 0.03 * \hat{C}_{init\ Bat\ ann}$
Annualized total cost	$\hat{C}_{Tot\ SC\ ann} = \hat{C}_{init\ SC\ ann} + \hat{C}_{rep\ SC\ ann} + \hat{C}_{main\ SC\ ann}$

Where  $\hat{C}_{inv\_PV}$  the investment cost of PV panels,  $\hat{C}_{inv\_FC}$  the investment cost of the FC,  $\hat{C}_{inv\_Bat}$  the investment cost of a battery,  $\hat{C}_{inv\_SC}$  the investment cost of SC bank and  $Pr_{m3\_H2}$  the price of one cubic meter of gaseous hydrogen. Unlike the rest of the components, the initial cost of PV panels includes a cost of installation and acquisition in addition to the purchase cost. Installation and acquisition costs are estimated at 40% of the purchase cost.

### C. Annualized total cost of the system

Finally, the total annualized cost of the system is given by (10):

$$\hat{C}_{Tot\_sys\_ann} = \hat{C}_{Tot\_PV\_ann} + \hat{C}_{Tot\_FC\_ann} + \hat{C}_{Tot\_Bat1\_ann} + \hat{C}_{Tot\_Bat2\_ann} + \hat{C}_{Tot\_Bat3\_ann} + \hat{C}_{Tot\_SC\_ann} \quad (10)$$

This cost represents the objective function to be optimized.

### D. Constraints of the problem

As explained in Section 3, the values of time horizons depend on the dynamics of the sources. For the generator 11, in order to avoid the negative values in the generated power (the FC is a unidirectional source) and also to obtain a smoothed profile, the horizon  $H_{11}^*$  must be wide. It is chosen to be of the order of days. Li-ion batteries are assumed to do a charge or discharge cycle in less than half a day. For this, horizons  $H_{21}^*$  and  $H_{22}^*$  are between 1 hour and 12 hours. The horizon  $H_{31}^*$  is of the order of minutes. This last choice is set after a set of tests that led us to conclude that if  $H_{31}^*$  is larger, the residual power ( $P_{SC}^*$ ) will not be well adapted to the capacity of the SC bank (too much energy). Concerning the coefficients, we consider that they must be positive to avoid the risk of reversing the sign of the power at the input of a filter (which causes charge instead of discharge and vice versa). The coefficient must also be less than 1 in order not to amplify the profiles at the input of the filters and consequently ask to supply or store an unnecessary power. Taking all this into account, the following constraints are defined:

$$1 \text{ day} \leq H_{11}^* \leq 15 \text{ days}$$

$$1 \text{ h} \leq H_{21}^*, H_{22}^* \leq 12 \text{ h}$$

$$5 \text{ min} \leq H_{31}^* \leq 15 \text{ min}$$

$$0.2 \leq a_{21}^*, a_{22}^*, a_{31}^* + a_{22}^* \leq 1$$

On stages 1 and 3, there is no power sharing in these two stages and therefore  $a_{11}^*$  and  $a_{31}^*$  are set at 1.

Added to that, the dimensions of ESS that will be given by the algorithm must respect the following constraints:

$$20\% \leq SoC_{Bat}(t) \leq 80\%, 0 \leq t \leq H_s \quad (11)$$

$$10\% \leq SoC_{SC}(t) \leq 100\%, 0 \leq t \leq H_s \quad (12)$$

Where  $SoC_{bat}(t) = -(1/E_{Bat}) \int P_{Bat}^* dt$   
 $E_{Bat}$  (J) represents the total energy of the battery.

$$\text{And } SoC_{SC}(t) = -(1/E_{SC\_Max}) \int P_{SC}^* dt$$

$$\text{Where } E_{SC\_Max} = (1/2)C_{SC}V_{SC\_Max}^2$$

$E_{SC\_Max}$  (J) the maximum energy that can be exchanged by the SC,  $C_{SC}$  (F) its total capacitance and  $V_{SC\_Max}$  (V) the maximum voltage at its terminals.

In fact, through the constraint (11), the deep charges/discharges are prevented because they accelerate the degradation of the batteries. On the other hand, SCs are

devices that support deep charges/discharges. The lower limit of the constraint (12) must be strictly positive in order not to generate an infinite current of the SC. It is fixed at 10%.

## V. SIMULATION RESULTS

Using the two estimated profiles cited in section 2, solving the previous optimization problem gives the following results:

Table 3. Optimization results.

$(H_{1,1}^*, a_{1,1}^*)$	(11.57 days, 1)
$(H_{2,1}^*, a_{2,1}^*)$	(11.98 h, 0.47)
$(H_{2,2}^*, a_{2,2}^*)$	(6.32 h, 0.53)
$(H_{3,1}^*, a_{3,1}^*)$	(6.66 min, 1)
Maximum power of the FC	343.4 W
Li-ion battery 1 min size	12008 Wh
Li-ion battery 2 min size	14677.5 Wh
Lead acid battery min size	6375 Wh
SC bank	$C_{SC}=50.65 \text{ F}$ , $P_{max}=3206 \text{ W}$

The power profiles associated to the previous values correspond to a total annualized cost of the system equal to 28044 €, in other words, equal to 7.25 € per kWh.

In a first simulation, it is assumed that the future estimates coincide perfectly with the powers actually measured. In this case, Figure 5a shows the evolution of  $P_{FC}^*$  over a day (in blue). The slow dynamics and the absence of sudden peaks and changes in power are the main characteristics of this profile. Figures 5b and 5c show the daily evolutions of the reference powers of Li-ion batteries (in blue). These two profiles are each characterized by the presence of two phases of charging and discharging each lasting about 12 hours. In fact, during the day, the batteries are charged by the excess of power that is created by solar panels. Figure 5d shows the daily power profile of lead-acid battery (in blue), which presents significant variations compared to those of Li-ion batteries. The figure 5e shows the residual power for the SC bank (in blue). It contains power peaks over very short periods of time, which means high powers and low energies.

Then, in a second simulation, forecasting errors are considered according to the equation (13). Indeed, future estimates of  $\Delta P$  are assumed to be lower than what will actually be measured:

$$\Delta P(t) = \hat{\Delta P}(t) + 10\% \hat{\Delta P}(t), 0 \leq t \leq H_s \quad (13)$$

Figure 5a shows the new power profile of the FC over a day (in red). This profile presents higher powers than those found in the first simulation, while keeping the same rate over time. This result is explained by equation (6), which reflects the evolution of  $P_{FC}^*$  over time. This new profile comes from the sum of the profile without FE (blue) and an averaged term of forecasting errors. As for the power profiles of the batteries and SC, the same phenomenon occurs. The reference powers of the three batteries and the SC bank are shown in the figures 5b, 5c, 5d and 5e respectively. Figure 6 shows the evolution of SoC of batteries and SC in both cases of simulation. In the presence of FE, SoCs exceeded safety limits because of the additional compensating powers. For this reason, the dimensions given by the optimization algorithm are the

minimum dimensions to use. In the sizing phase, forecasting errors should be taken into account.

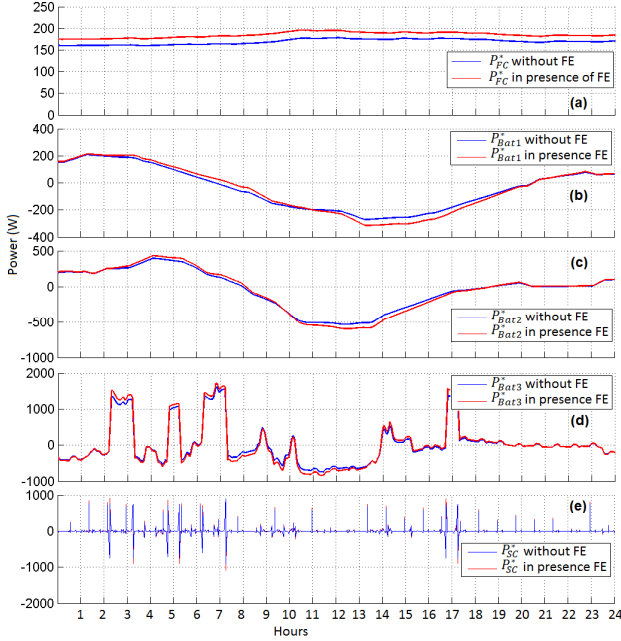


Fig. 5. Daily reference power profiles in presence of FE (red) and without FE (blue).

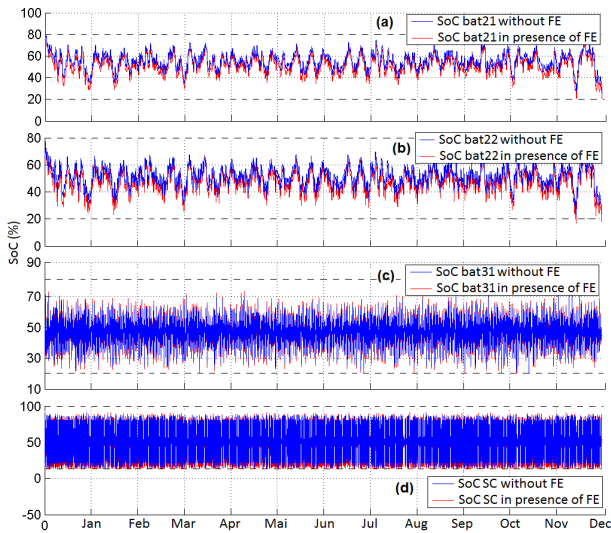


Fig. 6. Evolution of ESS's SoC in presence of FE (red) and without FE (blue).

## VI. CONCLUSION

This work presents an energy management strategy used to optimize energy distribution and sizes of the sources in a multisource production system feeding an isolated habitat. The studied system is composed of solar panels as a renewable source, a fuel cell, three batteries and a bank of supercapacitors as storage devices. It has a cascading architecture of several blocks called device-controllers, which operate mainly based on centered moving average filters coupled with safety and supervision functions. The proposed algorithm uses, as input data, a future estimate and also a measurement history of the load power and the photovoltaic power. In addition, the mathematical approach of the algorithm shows that it is able to compensate the forecasting

errors that can appear as a result of bad estimations. The simulation results showed the effectiveness of the proposed algorithm to respect the different power and energy constraints of the sources and also behaving with forecasting errors. As a perspective, the algorithm is to be generalized by adopting an architecture composed of 4 stages with  $N$  controllers per stage.

## REFERENCES

- [1] A. Bellaouar, A.S. Belleumi, "Fiabilité, maintenabilité, Disponibilité," university of Constantine 1, 2014.
- [2] Eng, J., He, H., & Xiong, R. "Rule based energy management strategy for a series-parallel plug-in hybrid electric bus optimized by dynamic programming," *Applied Energy*, 185, 1633-1643, 2016.
- [3] D. Arcos-Aviles, F. Guinjoan, P. M. Marietta, J. Pascual, L. Marroyo, and P. Sanchis, "Energy management strategy for a grid-tied residential microgrid based on fuzzy logic and power forecasting," *IECON 2016*, pp. 1-6, 2016.
- [4] O. Erdinc, B. Vural, and M. Uzunoglu, "A wavelet-fuzzy logic based energy management strategy for a fuel cell/battery/ultra-capacitor hybrid vehicular power system," *J. Power Sources*, vol. 194, no. 1, pp. 369-380, 2009.
- [5] Hredzak, B., & Agelidis, V. G. "Model predictive control of a hybrid battery-ultracapacitor power source," *Proceedings of The 7th International Power Electronics and Motion Control Conference*, 29(3), 2294-2299, 2012.
- [6] O. Erdinc, B. Vural, and M. Uzunoglu, "A wavelet-fuzzy logic based energy management strategy for a fuel cell/battery/ultra-capacitor hybrid vehicular power system," *J. Power Sources*, vol. 194, no. 1, pp. 369-380, 2009.
- [7] S. Bourdim, T. Azib, K. E. Hemsas, C. Larouci, E. Departement, and C. A. Hamani, "Efficient Energy Management Strategy for Fuel Cell Ultracapacitor Hybrid System," *ESARS-ITEC*, pp. 1-6, 2016.
- [8] M. Uzunoglu, M.S. Alam, Modeling and analysis of an FC/UC hybrid vehicular power system using a novel wavelet based load sharing algorithm, *IEEE Trans Energy Conversion* 23 (1) (2008) 263-272.
- [9] A. Bouabdallah, J. C. Olivier, S. Bourguet, A. Houari and M. Machmoum, "Robust sizing of a stand alone multi-sources power system," *Industrial Technologie (ICIT)*, 448-453, 2016.
- [10] Pascual, J., Barricarte, J., Sanchis, P., & Marroyo, L. "Energy management strategy for a renewable-based residential microgrid with generation and demand forecasting," *Applied Energy*, 158, 12-25, 2015.
- [11] Sang C. Lee & Woo Young Jung, «Analogical understanding of the Ragone plot and a new categorization of energy devices», *Energy procedia*, pp. 526-530, 2016.
- [12] C. Depature, S. Jemei, L. Boulon, A. Bouscayrol, N. Marx, S. Morando, and A. Castaigns, "IEEE VTS Motor Vehicles Challenge 2017 - Energy Management of a Fuel Cell/Battery Vehicle," 2016 *IEEE Veh. Power Propuls. Conf. VPPC 2016 - Proc.*, 2016.
- [13] W. Zhang, J. Li, L. Xu, and M. Ouyang, "Optimization for a fuel cell/battery/capacity tram with equivalent consumption minimization strategy," *Energy Convers. Manag.*, vol. 134, pp. 59-69, 2017.
- [14] S. Hmam, J. C. Olivier, S. Bourguet, and L. Loron, "A cycle-based and multirate approach for power system simulation application to the ageing estimation of a supercapacitor-based ferry," *J. Energy Storage*, vol. 8, pp. 175-184, 2016.
- [15] S. Trieste, S. Hmam, J. C. Olivier, S. Bourguet, and L. Loron, "Techno-economic optimization of a supercapacitor-based energy storage unit chain: Application on the first quick charge plug-in ferry," *Appl. Energy*, vol. 153, pp. 3-14, 2015.
- [16] Saidi, R., Olivier, J. C., Chauveau, E., & Machmoum, M. "Energy Management Strategy for Hybrid Power Systems based on Moving Average Filters and Power Forecasting", *ICIT, Lyon*, 2018.
- [17] Saidi, R., Olivier, J. C., Chauveau, E., & Machmoum, M. « Méthode générique de gestion de l'énergie des systèmes multisources par filtres à moyenne glissante », *SGE, Nancy*, 2018.